Characterisation of fatigue crack growth using digital image correlation measurements of plastic CTOD

J.M. Vasco-Olmo, F.A. Díaz, F.V. Antunes, M.N. James

PII: S0167-8442(18)30655-4
DOI: https://doi.org/10.1016/j.tafmec.2019.03.009
Reference: TAFMEC 2215

To appear in: *Theoretical and Applied Fracture Mechanics*

Received Date: 20 December 2018
Revised Date: 14 March 2019
Accepted Date: 15 March 2019

Please cite this article as: J.M. Vasco-Olmo, F.A. Díaz, F.V. Antunes, M.N. James, Characterisation of fatigue crack growth using digital image correlation measurements of plastic CTOD, *Theoretical and Applied Fracture Mechanics* (2019), doi: https://doi.org/10.1016/j.tafmec.2019.03.009

Characterisation of fatigue crack growth using digital image correlation measurements of plastic CTOD

J.M. Vasco-Olmo[1*], F.A. Díaz[1], F.V. Antunes[2], M.N. James[3, 4]

[1]Departamento de Ingeniería Mecánica y Minera, University of Jaén, Jaén, Spain.

[2]Department of Mechanical Engineering, University of Coimbra, Coimbra, Portugal.

[3]School of Engineering, University of Plymouth, Plymouth, United Kingdom.

[4]Department of Mechanical Engineering, Nelson Mandela Metropolitan University, Port Elisabeth, South Africa.

*corresponding author: jvasco@ujaen.es

Abstract. Crack tip opening displacement (CTOD) was measured using digital image correlation (DIC) and resolved into elastic and plastic CTOD components via an offset compliance technique. The plastic CTOD range gave a single linear correlation for fatigue crack growth rate at stress ratios of 0.1 and 0.6 in compact-tension (CT) specimens of Grade 2 titanium. A sensitivity analysis was performed to find the optimum position in the crack wake to make the CTOD measurements. The results are the first time (to the authors knowledge) that plastic CTOD has been found directly from experimentation and demonstrate that plastic CTOD is a useful alternate characterising parameter for fatigue crack growth to the stress intensity factor defined by Irwin.

Keywords: Crack tip opening displacement (CTOD), fatigue crack growth rate, DIC, range of plastic CTOD.

Nomenclature:

CCD:	charge-coupled device camera
CJP:	Christopher-James-Patterson model of crack tip fields
COD:	crack opening displacement
CT:	compact-tension specimen
CTOD:	crack tip opening displacement
$CTOD_{el}$:	elastic component of crack tip opening displacement
$CTOD_{exp}$:	experimental value of crack tip opening displacement
$CTOD_{p}$:	plastic component of crack tip opening displacement
$CTOD_{t}$:	total crack tip opening displacement
$CTOD_{th}$:	theoretical value of crack tip opening displacement
da/dN:	fatigue crack growth rate
DIC:	digital image correlation technique
LEFM:	linear elastic fracture mechanics
L_x:	direction along the crack plane for the CTOD measurement
L_y:	direction perpendicular to the crack for the CTOD measurement
MT:	middle-tension specimen
R:	ratio between the minimum and maximum applied load in fatigue
ΔCMOD:	range of crack mouth opening displacement
ΔCTOD:	range of crack tip opening displacement
$\Delta CTOD_{t}$:	range of total crack tip opening displacement
$\Delta CTOD_{el}$:	range of elastic crack tip opening displacement
$\Delta CTOD_{p}$:	range of plastic crack tip opening displacement
ΔJ:	cyclic J-integral
ΔK:	range of stress intensity factor

1. Introduction

Under nominally small-scale yielding conditions, where the extent of nonlinear plastic deformation at the tip of a growing fatigue crack is small enough that the overall response of the body remains elastic, the crack growth rate can be related to the applied stresses using the so-called Paris 'law' where the characterising parameter is the range of elastic stress intensity factor [1],[2]. Although the Paris law provides a useful and successful characterisation of fatigue crack growth rate in many engineering applications, it suffers from the major deficiency of being purely empirical, and hence provides no fundamental insight into the mechanisms of fatigue crack propagation.

This point was noted by Hosseini et al. [3] and has led to ongoing difficulties in situations where the LEFM similitude concept breaks down, in particular in situations where plasticity-induced fatigue crack closure or crack tip shielding mechanisms operate. The CJP model for crack tip stress and displacement fields [4] – [6] deals with this problem of lack of physical insight by defining a modified set of stress intensity factors that directly characterise the effective driving force for fatigue crack growth in the presence of a plastic enclave surrounding the growing fatigue crack. These incorporate several effects of the plasticity-induced forces acting at the elastic-plastic boundary, e.g. crack wake contact and compatibility-induced shear stresses acting in the plane of the crack, and hence have the capability of providing physical insight into mechanisms. This approach has proven to be very useful in quantifying plastic zone size and shape [7] and in better rationalising fatigue crack growth rate data across different specimen geometries and stress ratios [8], than the traditional Irwin definition of stress intensity factor.

Ritchie and co-workers provide a very useful summary of the various more analytical attempts at modelling fatigue crack growth rate [3], pointing out that a sound description of the stress and strain fields ahead of a propagating fatigue crack, based on appropriate constitutive equations, has been lacking (the CJP model is a crack tip field model that incorporates elastic stresses induced by the plastic enclave and does not consider the overall constitutive relationships). Reference [3] goes on to derive a constitutive law for cyclic plasticity and then uses finite element modelling to calculate the plasticity-driven crack propagation rate under cyclic loading. The steady-state growth rate *da/dN* is calculated by considering the change in location of the crack tip during a load cycle, with the magnitude of the growth rate reflecting the plastic state of

the material ahead of the crack tip and the associated plastic energy dissipation. The work in reference [3] provides an underpinning constitutive model for the use of crack tip opening displacement (CTOD) to characterise fatigue crack growth rate.

The CTOD parameter was originally proposed by Wells [9] and Burdekin and Stone [10] as a more physically-based explanation for crack extension processes that could be related to the crack tip blunting explanation of fatigue crack growth and striation formation given by Laird and Smith [11]. The CTOD concept has been quite widely applied in characterisation of fatigue crack growth rate. Donahue et al. [12] reported that fatigue crack growth data for a wide variety of different materials could be accurately described in terms of the mechanical properties and two material constants, one of which was the threshold stress intensity factor, by using a direct proportionality between the rate of fatigue crack growth and crack opening displacement (COD). Nicholls [13] assumed a polynomial relationship between crack blunting and crack extension to derive an expression for the rate of fatigue crack growth. His expression accurately predicted fatigue crack growth rates for a wide variety of titanium, nickel, aluminium and steel alloys. Shahani et al. [14] presented several equations to describe fatigue crack growth rates, via ΔJ, ΔCTOD, ΔCMOD and ΔK. Their experimental results indicated that ΔJ and ΔCTOD varied with the stress ratio (R) and were better parameters for characterising fatigue crack growth rate than ΔCMOD and ΔK, which were constant with R.

Yates, Zanganeh and Tai [15] provided an overview of some applications of DIC in characterising full-field elastic-plastic crack tip displacement fields. In recent years DIC has been applied across a range of cracking-related issues, including determination of crack opening profiles and CTOD [16], low cycle fatigue [17] and correlating fatigue crack growth rates [18]. Deng et al. [17] estimated cyclic CTOD for low-cycle failure analysis on a central-through cracked plate made of Q235 steel by using the plastic strain accumulation at the crack tip as the controlling parameter. They observed that plastic strain accumulates in the local crack tip field, eventually stabilising with increase in cycling time. Dong et al. [18] proposed an analytical model that gave a linear correlation between da/dN and ΔCTOD, concluding that CTOD was able to characterise the crack tip state in large scale yielding. They found a good correlation between predictions and experimental results, which showed that the crack opening displacement was able to characterise the crack tip state for constant amplitude fatigue

crack growth with large scale yielding. Their study also considered the influence of crack closure arising from the plastic wake left behind the crack tip.

CTOD has also been widely invoked in finite element numerical models of fatigue crack growth rate, with early work by Gu and Ritchie [19] modelling plasticity-driven crack propagation of a blunted crack under cyclic loading, based on crack-tip blunting without the need to introduce any specific failure criterion. This was subsequently confirmed by Tvergaard [20] who extended the work by incorporating a re-meshing technique and was hence able to model plasticity-driven crack growth over several hundred loading cycles. In more recent work, Antunes et al. [21] note that the experimental determination of crack tip opening displacement, CTOD, can be difficult due to the relatively small displacements involved, and that numerical or analytical techniques have been more usually employed in investigating the relationship between CTOD and fatigue crack growth rate. In this respect, the paper by Korsunsky et al. [22] provides a useful overview of experimental and modelling studies of fatigue crack growth rates in Ti-6Al-4V alloy. The work by Antunes et al. [21] was concerned with improving the understanding of crack closure and fatigue crack growth rate using CTOD, through studying phenomena such as crack flank contact, crack opening, and elastic and plastic deformation. They obtained a polynomial relationship between *da/dN* and the plastic CTOD for their 6082-T6 aluminium alloy independent of the stress ratio, supporting the view that CTOD is a more physically meaningful alternative to ΔK in analysing fatigue crack propagation.

Experimental DIC studies of CTOD are relatively few in number, although recent papers have considered the application of DIC in such diverse areas as crack closure in low cycle fatigue [23], [24], experimental macro- and micro-measurement of near-tip displacement fields at uniform and variable loading [25] and due to single overloads and underloads [26], and surface cracks [27], as well as developing more efficient algorithms for mathematical processing of the experimental displacement fields obtained by DIC [28]. The present work applies DIC to quantifying values of the plastic CTOD in order to confirm whether a linear relationship can be obtained between fatigue crack growth, *da/dN*, and $\Delta CTOD_p$, independent of the applied stress ratio in the fatigue cycling, and to demonstrate that DIC techniques can now achieve the required resolution for such experiments. Note that the values of $\Delta CTOD_p$ reported in [21] from finite element analysis are relatively small (<1 μm) which presents a

challenge for experimental determination of the plastic CTOD. In this respect, Korsunsky et al. [22] noted in 2009 that although DIC techniques held out the promise of sub-micron spatial resolution, published results pertained primarily to the extraction of global parameters, due to generally insufficient accuracy to quantify strain distributions. In the present research, DIC was applied to fatigue cracks growing in Grade 2 commercially pure titanium at stress ratios of 0.1 and 0.6. The CTOD was measured from the relative vertical displacements between the crack flanks.

2. Experimental details

Two CT specimens (dimensions shown in Figure 1a) were manufactured from a 1 mm thick sheet of commercially pure Grade 2 titanium and tested in constant amplitude fatigue loading with a maximum load of 750 N at stress ratio values of 0.1 and 0.6. The specified chemical composition for Grade 2 titanium is presented in Table 1 and compared with measured values, while Table 2 presents the measured tensile data.

The two surfaces of each specimen were treated using different methods to enable simultaneous measurements of the displacement field by digital image correlation (DIC) on one side and crack length on the other. The surface used for the DIC study was sprayed with a random black speckle pattern over a white background (see Figure 1b), while the other surface of the specimen was ground and polished to allow tracking of the crack tip position with a macro-zoom lens (MLH-10X EO).

Fatigue tests were conducted on an Electropuls E3000 electrodynamic machine (Figure 2) at a loading frequency of 10 Hz. A CCD camera, fitted with a macro-zoom lens similar to that indicated above to increase the spatial resolution at the region around the crack tip, was placed perpendicularly to each face of the specimen. During fatigue testing, the cyclic loading was periodically paused to allow acquisition of a sequence of images at uniform increments through a complete loading and unloading cycle. The CCD camera viewing the speckled surface of the specimen was set up so that the field of view was 17.3 x 13 mm (resolution of 13.7µm/pixel) with the crack path located at the centre of the image. A fibre optic ring placed around the zoom lens provided illumination of the specimen surface (also shown in Figure 2).

3. Methodology for locating the crack tip

As indicated above, CTOD is a parameter that measures the opening at the crack tip, hence the vertical displacements obtained from experiments are used in analysing its

value. Examples of DIC horizontal and vertical displacement maps for a crack length of 9.40 mm and a load level of 750 N are shown in Figure 3. The method of obtaining the CTOD from measurements of the relative displacement between the crack flanks of selected points behind the crack tip is explained below. It is important to note that the accuracy of the results is strongly influenced by location of the assumed crack tip; accurate location is therefore important and this is found in the following manner. Firstly, the *y*-coordinate of the crack tip is found by plotting a set of profiles of vertical displacement perpendicular to the crack plane as all profiles converge onto a single point where they cross the crack plane. This is clearly seen in Figure 4a and the intersection point identifies the location of the crack tip in the *y*-direction. The corresponding vertical displacement *y*-coordinate for this point is marked in Figure 4a because it is then used to find the *x*-coordinate of the crack tip. This is done by plotting a displacement profile in the x-direction, parallel with the crack direction, and locating the point that corresponds with the same displacement value (v = 0.158 mm) previously found for the *y*-coordinate (Figure 4b). Using this procedure, the crack tip was identified as located at the point with coordinates x = 470 pixels and y = 468 pixels, with the coordinate origin being at the upper left corner of the vertical displacement map (Figure 3b).

Once the crack tip location is established, the CTOD can be obtained by defining a suitable pair of measurement points behind the crack tip, and determining the CTOD through a complete loading cycle by analysing both the loading and unloading half cycles. From this information, the portion of the cycle during which the crack is nominally closed or open can be found. Finally, from analysis of the portion of the load cycle during which the crack is open, both the elastic and plastic components of the CTOD can be estimated from the variation in slope observed in the CTOD versus load curves.

4. Effect of the position behind the crack tip

A sensitivity analysis was performed to explore the influence of the distance behind the crack tip of the pair of points selected for the CTOD measurements, as this is clearly critical to interpreting CTOD data and correlating it with fatigue crack growth rate. The position of these two points behind the crack tip is given in Figure 5 as L_x in the direction of the crack plane and L_y in the direction perpendicular to the crack. The

coordinate axes have been modified establishing their origin at the coordinates found in the previous section for the crack tip.

The sensitivity analysis involved measuring the CTOD at the maximum load as a function of one of the parameters, whilst maintaining the other one fixed. Figure 6 presents the results of this analysis, with Figure 6a plotting the CTOD as a function of L_x for various value of L_y and Figure 6b giving it as a function of L_y for different values of L_x. As would be expected, CTOD values increase steadily with increasing distance behind the crack tip. The key observation from these data considering Figure 6a is that for any particular L_y value >10 pixels (136.9 μm) the CTOD reaches an upper bound limit for L_x distances behind the crack tip approximately ≥ 120 μm. This is more clearly shown in Figure 6b where for L_x values approximately > 8 pixels (82.1 μm) the CTOD value attains a plateau at a L_y distance of approximately 140 μm. This stable plateau region is the result of rigid body motion and indicates the boundary of the region undergoing crack tip deformation and its onset can hence be used to characterise the CTOD. The plateau region is indicated with the rectangle in Figure 6b and encloses the CTOD values corresponding to the ranges 5–15 pixels (68.4–205.3 μm) for L_x and 10–15 pixels (136.8–205.3 μm) for L_y. This analysis demonstrates that the CTOD is accurately characterised by using data corresponding with the position of two points with a horizontal position L_x = 5 pixels (68.4 μm) and vertical position L_y = 10 pixels (136.8 μm) behind the crack tip.

5. Experimental results

Once the values of L_x and L_y were established, the CTOD through a loading cycle for any particular crack length could be obtained from analysis of the DIC data. A typical plot showing CTOD at increments of 25 N throughout a full loading cycle for a crack length of 9.40 mm in the case of the specimen tested at R = 0.1 and a crack length of 9.20 mm in the case of the specimen tested at R = 0.6 is shown in Figure 7. The elastic and plastic CTOD values can be obtained from the data given in Figure 7, using an offset procedure similar to that reported by Skorupa et al. [29] for compliance measurements. In this process, a least squares straight line was fitted to experimental data over the part of the load cycle that corresponds with elastic deformation (see lines drawn in Figure 7). The elastic portions of the loading cycle were identified using a 3 point sliding average, founding a range between 15% and 55% of the loading range from the minimum applied load for the specimen tested at R = 0.1 and between the minimum applied load and a 40% of the loading range from the minimum load for the

specimen tested at R = 0.6. To evaluate how the components of CTOD can change depending on the loading range selected, a sensitivity analysis was performed to evaluate the errors made when variations of ±10% for the lower and upper limits are analysed. According to this sensitivity analysis, the variations of the lower limit involved errors between 3–4% for the plastic CTOD and 1.0–1.5% for the elastic component. On the other hand, the variations on the upper limit involved errors between 6.5–10% for the plastic CTOD and 3–4.5% for the elastic CTOD. From these results it is evident that the selection of the upper limit is more restrictive than the lower limit. This is not strange since the upper limit establishes the separation between the elastic and plastic components. Therefore, these results obtained from the sensitivity analysis strengthen the definition of the loading range for describing the elastic behaviour. The equation obtained from this linear fit was employed to calculate the theoretical CTOD value corresponding to all analysed load levels. Thus, the CTOD offset was obtained from Eq. (1). The ranges of the elastic and plastic components of the CTOD can then be defined as shown in Figure 7.

$$CTOD\,offset = \frac{CTOD_{th} - CTOD_{exp}}{CTOD_{th}} \cdot 100 \tag{1}$$

The CTOD offset is plotted against applied load (Figure 8) and the elastic region is determined in accordance with the standard E 647 [30], where a CTOD change of 4% either side of the zero value is taken as representing the offset criterion (marked in Figure 8 and corresponding with a compliance change of ≈4%) and establishes the elastic region in the offset CTOD trace. The letters *A* to *D* in Figures 7a and 8a define the various regions in the CTOD loading cycle for the specimen tested at R = 0.1, where the load range between *B* and *C* (175 N to 450 N) defines elastic behaviour. It is clear in Figure 7a that from point *C* there is a deviation from linearity up to point *D*, corresponding to the maximum applied load, and this is attributed to plastic deformation. The elastic and plastic ranges of CTOD can then be estimated by extrapolating the linear regime to the maximum load (Figure 7). During unloading, there is a linear decrease in CTOD between points *D* and *E* with the same slope than that obtained for the elastic regime in the loading half cycle. As is the case for the loading half cycle, there is a change in the linearity during further unloading due to the reversed plastic deformation.

The elastic and plastic ranges of CTOD during the loading half cycle were therefore obtained from Figure 7a as 13 μm and 6 μm, respectively and the corresponding

values for the unloading half cycle were 13.2 μm and 5.8 μm, respectively. The plastic CTOD is hence 31.6% (loading) and 30.5% (unloading) of the maximum CTOD. The region between points *A* and *B* in Figures 7a and 8a is associated with crack opening and closing and additional work could be done to estimate the opening and closing loads; however, any additional information gained on the subjects of crack closure and crack tip shielding is both complex in interpretation of its true effects, and is not germane to the present study.

Similar procedure can be extrapolated in the case of the specimen tested at R = 0.6 but with the difference that the loading range is between 450 N and 750 N. The elastic and plastic ranges of CTOD were 8.7 μm and 2.9 μm, respectively. It is clear the difference between these values and those obtained for R = 0.1. However, these values are coherent since the loading range for the test at high ratio is a 44% of that corresponding to the low ratio. Another important difference respect the CTOD plot at low R-ratio is that the region between *A* and *B* point was not identified. This is not surprising since at R = 0.6 any crack shielding effect was not expected.

The methodology described above to obtain the CTOD range for the elastic and plastic components was applied to data recorded during crack growth for the tests conducted at the stress ratios of R = 0.1 and 0.6. Figure 9a shows the elastic and plastic CTOD data as a function of crack length. Significant scatter is observed in the elastic CTOD values, being those at R = 0.6 about a half of those values at R = 0.1; while those representing the plastic CTOD show a more consistent increment with increase in crack length. Plastic CTOD demonstrates a faster rate of increase at R = 0.1 than at R = 0.6. However, normalising the elastic and plastic ranges of CTOD values by the total range of CTOD gives a much more uniform picture at the two stress ratio values (Figure 9b) and the data for the elastic CTOD now shows more consistent behaviour. The trends in the CTOD curves in Figure 9b appear sensible since, as the crack is propagating, the plastic deformation is increasing and, with it, the plastic CTOD, whilst the value of the elastic CTOD undergoes a corresponding decrease as a percentage of the total CTOD.

Figure 10 presents data for da/dN as a function of the ranges of $CTOD_t$, $CTOD_{el}$ and $CTOD_p$ for the specimen tested at R = 0.1. It is clear that only the plastic component of CTOD shows a consistent increase with crack growth rate and could therefore be used

to characterise fatigue crack growth rate. Figure 11 shows the *da*/*dN* versus $\Delta CTOD_p$ curves obtained at both R = 0.1 and 0.6 that demonstrate a very good correlation of fatigue crack growth rate into a single linear relationship. It should be noted that this correlation is obtained without employing logarithmic scales as is necessary when using the Paris law. The crack growth rate is then given by linear regression as:

$$\frac{da}{dN} = 0.2706 \times \Delta CTOD_p \quad (2)$$

The constant in Eq. (2) does not have units, unlike the constants defined by Paris law, and a linear relationship between *da/dN* and the range of CTOD was also observed by Guo et al. [31], Tvergaard [20] and Pippan and Grosinger [32]. Those works, however, all used the total CTOD and they did not distinguish between the plastic and elastic CTOD components. A linear relationship between *da/dN* and $\Delta CTOD_p$ has been reported by Antunes et al. [33] in work on 7050-T6 aluminium alloy that combined numerical modelling and experimental data in recently published work. They obtained *da/dN* data from experiments in middle-tension (MT) specimens for different stress ratios while the plastic CTOD data were numerically determined by using the methodology previously reported in [21]. They obtained the relationship *da/dN* = 0.5246 x $\Delta CTOD_p$.

In contrast, in the experimental work presented here, *da/dN* data were obtained from measurements of crack length and number of cycles, with the CTOD data obtained from analysis of DIC measurements of the vertical displacement. To the knowledge of the present authors, this is the first time that plastic CTOD data, determined solely by experimentation, has been used to characterise fatigue crack growth rate at two different stress ratio values.

6. Conclusions

The plastic range of CTOD is clearly linked with the plastic deformation generated at the crack tip during fatigue crack propagation at constant amplitude. The range of plastic CTOD ($\Delta CTOD_p$) has therefore been used to characterise and correlate fatigue crack growth data obtained at two different stress ratio values of 0.1 and 0.6. A linear relationship between *da/dN* and $\Delta CTOD_p$, independent of stress ratio was, observed for a CP titanium alloy. The CTOD was measured from the relative vertical displacement between the crack flanks. A sensitivity analysis was performed to determine the optimum position behind the crack tip of the points where displacement

was measured, and it was found that the CTOD value showed a significant dependence on their location in the plane of the crack. However, the influence of the vertical distance from the crack plane was not as restrictive, with a stable value of CTOD being obtained at a distance of 136.9 μm. This conclusion was reached using a methodology that analysed different displacement profiles plotted from the vertical displacement map.

This work has demonstrated that CTOD represents a viable alternative technique to stress intensity factor in characterising fatigue crack growth rate since CTOD considers fatigue threshold and crack shielding in an intrinsic way [33]. However, further work is necessary to determine whether the linear relationship observed between *da/dN* and $\Delta CTOD_p$ may be considered as an intrinsic material property, independent of the geometry and loading conditions. The plastic CTOD approach is, however, unlikely to shed light on the physical mechanisms underlying such phenomena as plasticity-induced crack tip shielding and a combination of approaches will be required to advance understanding, e.g. the use of plastic CTOD and the CJP model of crack tip fields.

Acknowledgements

This work has been conducted with financial support from Gobierno de España through the project “Proyecto de Investigación de Excelencia del Ministerio de Economía y Competitividad MAT2016-76951-C2-1-P”.

References

[1] Gomez M.P., Anderson, W.E., A rational theory of fatigue. Trend Engineering, 1961. **13**: p. 9-14.

[2] Paris, P., Erdogan, F., A critical analysis of crack propagation laws. Journal of Basic Engineering, 1963. **85**(4): p. 528-534.

[3] Hosseini, Z.S., et al., On the theoretical modeling of fatigue crack growth. Journal of the Mechanics and Physics of Solids, 2018. **121**: p. 341-362.

[4] James, M.N., et al., Local crack plasticity and its influences on the global elastic stress field. International Journal of Fatigue, 2013. **46**: p. 4-15.

[5] Christopher, C.J., et al., Towards a new model of crack tip stress fields. International Journal of Fracture, 2008. **148**(4): p. 361-371.

[6] Vasco-Olmo, J.M., et al., Crack tip plastic zone evolution during an overload cycle and the contribution of plasticity-induced shielding to crack growth rate changes. Fatigue and Fracture of Engineering Materials and Structures, 2018. **41**: p. 2172-2186.

[7] Vasco-Olmo, J.M., et al., Assessment of Crack Tip Plastic Zone Size and Shape and its Influence on Crack Tip Shielding. Fatigue & Fracture of Engineering Materials & Structures, 2016. **39**(8): p. 969-981.

[8] Yang, B., et al., A more effective rationalisation of fatigue crack growth rate data for various specimen geometries and stress ratios using the CJP model. International Journal of Fatigue, 2018. **114**: p: 189-197..

[9] Wells, A.A. Unstable Crack Propagation in Metals-Cleavage and Fast Fracture. in Crack Propagation Symposium. 1961. Cranfield: College of Aeronautics, Cranfield.

[10] Burdekin, F.M., Stone, D.E.W., The Crack-Opening-Displacement Approach to Fracture Mechanics in Yielding. Journal of Strain Analysis, 1966. **1**(2): p. 145-153.

[11] Laird, C., Smith, G.C., Crack propagation in high stress fatigue. The Philosophical Magazine: A Journal of Theoretical Experimental and Applied Physics, 1962. **7**(77): p. 847-857.

[12] Donahue, R.J., et al., Crack opening displacement and the rate of fatigue crack growth. International Journal of Fracture Mechanics, 1972. **8**(2): p. 209-219.

[13] Nicholls, D.J., The relation between crack blunting and fatigue crack growth rates. Fatigue & Fracture of Engineering Materials & Structures, 1994. **17**(4): p. 459-467.

[14] Shahani, A.R., et al., A unified model for the fatigue crack growth rate in variable stress ratio. Fatigue & Fracture of Engineering Materials & Structures, 2009. **32**(2): p. 105-118.

[15] Yates, J.R., Zanganeh, M., Tai, Y.H., Quantifying crack tip displacement fields with DIC. Engineering Fracture Mechanics, 2010. **77**(11): p. 2063-2076.

[16] Tagawa, T., et al., Experimental measurements of deformed crack tips in different yield-to-tensile ratio steels. Engineering Fracture Mechanics, 2014. **128**: p. 157-170.

[17] Deng, J., et al., Research on CTOD for low-cycle fatigue analysis of central-through cracked plates considering accumulative plastic strain. Engineering Fracture Mechanics, 2016. **154**: p. 128-139.

[18] Dong, Q., et al., Mechanisms and modeling of low cycle fatigue crack propagation in a pressure vessel steel Q345. International Journal of Fatigue, 2016. **89**: p. 2-10.

[19] Gu, I., R.O. Ritchie, On the crack-tip blunting model for fatigue crack propagation in ductile materials. ASTM Special Technical Publication, 1999(1332): p. 552-564.

[20] Tvergaard, V., On fatigue crack growth in ductile materials by crack–tip blunting. Journal of the Mechanics and Physics of Solids, 2004. **52**(9): p. 2149-2166.

[21] Antunes, F.V., et al., A numerical analysis of CTOD in constant amplitude fatigue crack growth. Theoretical and Applied Fracture Mechanics, 2016. **85**: p. 45-55.

[22] Korsunsky, A.M., et al., Crack tip deformation fields and fatigue crack growth rates in Ti–6Al–4V. International Journal of Fatigue, 2009. **31**(11): p. 1771-1779.

[23] Rabbolini, S., Beretta, S., Foletti, S., Fatigue crack growth in low cycle fatigue: an analysis of crack closure based on image correlation. Procedia Structural Integrity, 2016. **1**: p. 158-165.

[24] Patriarca, L., Foletti, S., Beretta, S., A comparison of DIC-based techniques to measure crack closure in LCF. Theoretical and Applied Fracture Mechanics, 2018. **98**: p. 230-243.

[25] O'Connor, S.J., Nowell, D., Dragnevski, K.I., Measurement of fatigue crack deformation on the macro- and micro-scale: uniform and non-uniform loading. International Journal of Fatigue, 2016. 89: p. 66-76.

[26] Eremin, et al., DIC study of fatigue crack growth after single overloads and underloads, Procedia Structural Integrity, 2017. 5: 889-895.

[27] Samadian, K., Hertelé, S., De Waele, W., Measurement of CTOD along a surface crack by means of digital image correlation. Engineering Fracture Mechanics, 2019. **205**: p. 470-485.

[28] Chernyatin, A.S., et al., Multi-approach study of crack-tip mechanics on aluminium 2024 alloy. Theoretical and Applied Fracture Mechanics, 2018. **98**: p. 38-47.

[29] Skorupa, M., et al., An algorithm for evaluating crack closure from compliance measurements. Fatigue & Fracture of Engineering Materials & Structures, 2002. **25**: p. 261-273.

[30] ASTM, E647 Standard Test Method for Measurement of Fatigue Crack Growth Rates. 2015, American Society for Testing and Materials: Philadelphia, PA.

[31] Guo, W., Wang, C.H., Rose, L.R.F., The influence of cross-sectional thickness on fatigue crack growth. Fatigue & Fracture of Engineering Materials & Structures, 1999. **22**(437-444).

[32] Pippan, R.G., Grosinger, W., Fatigue crack closure: From LCF to small scale yielding. International Journal of Fatigue, 2013. **46**: p. 41-48.

[33] Antunes, F.V., et al., Fatigue crack growth modelling based on CTOD for the 7050-T6 alloy. Fatigue & Fracture of Engineering Materials & Structures, 2017. **40**: p. 1309-1320.

Tables

Table 1 Chemical composition of commercially pure titanium Grade 2.

Element (wt %)	Fe	C	N	O	H	Titanium
Requirement	<0.20	≤0.08	≤0.05	≤0.20	≤0.015	Balance
Result	0.10	0.01	<0.01	0.12	0.002	Balance

Table 2 Measured mechanical properties.

Parameter	E (GPa)	UTS (MPa)	σ_{ys} (MPa)	ε_f (%)	v
Value	105	448	390	20	0.33

Figures

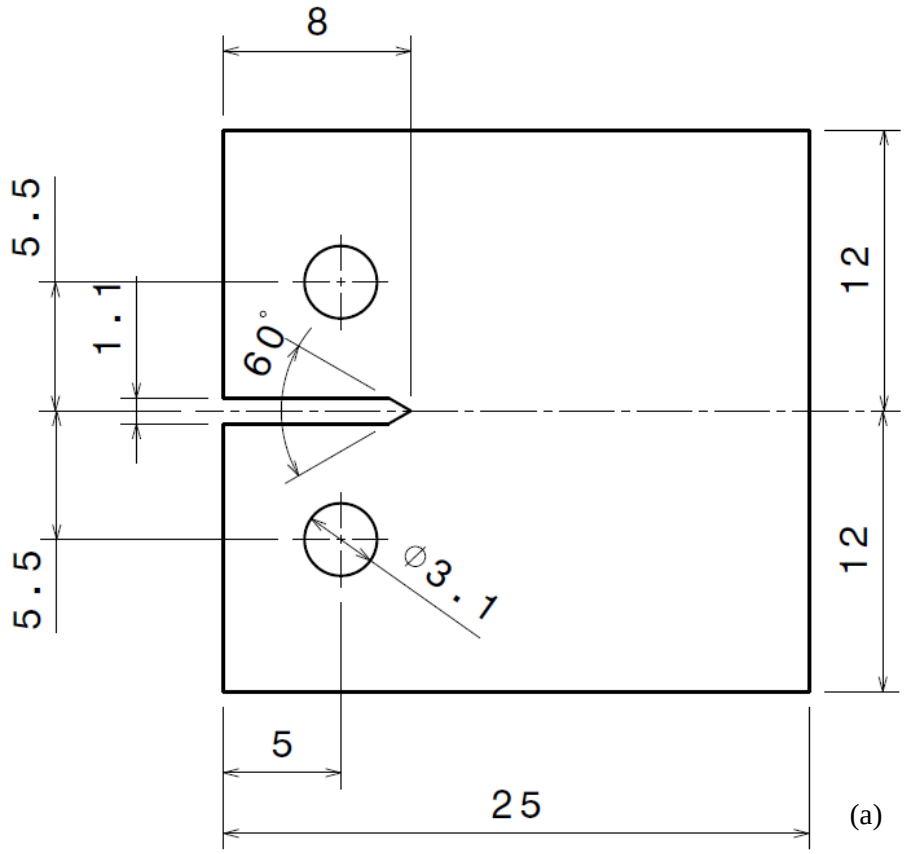

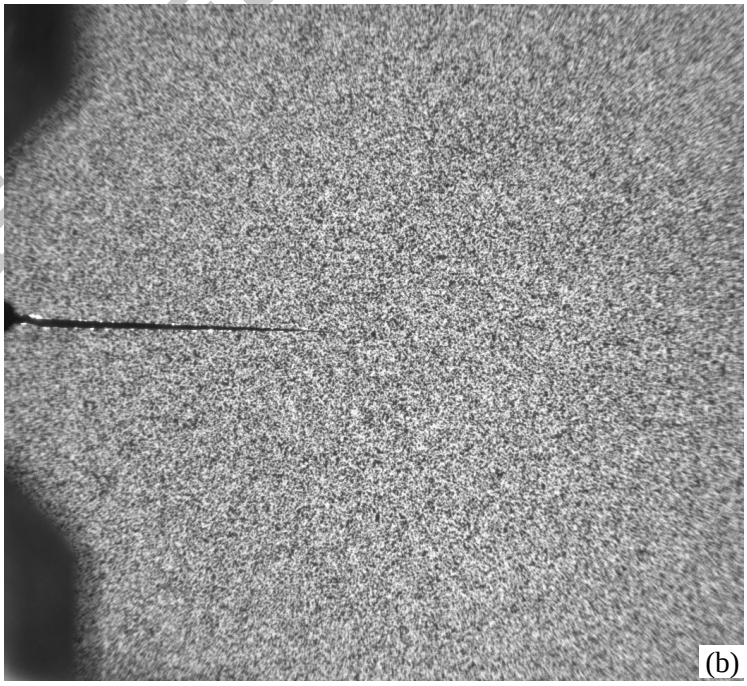

Figure 1 a) Dimensions of the CT specimens (mm). (b) Illustration of the speckle pattern sprayed onto the specimen surface for making DIC measurements.

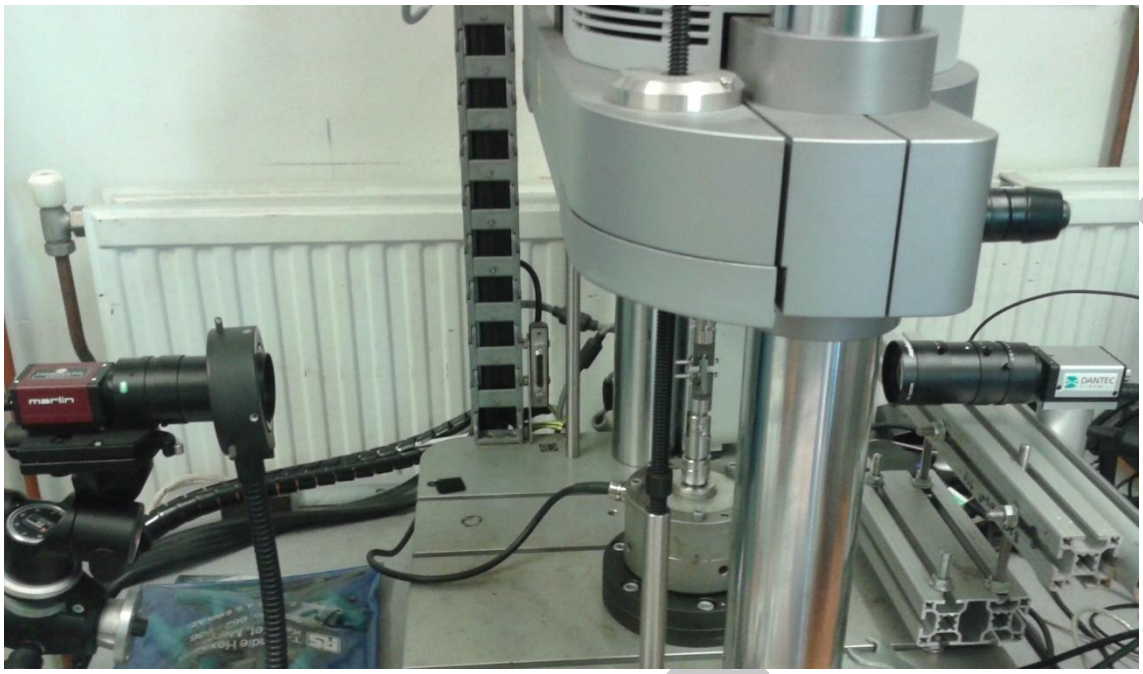

Figure 2 Experimental set-up used for fatigue testing and data acquisition.

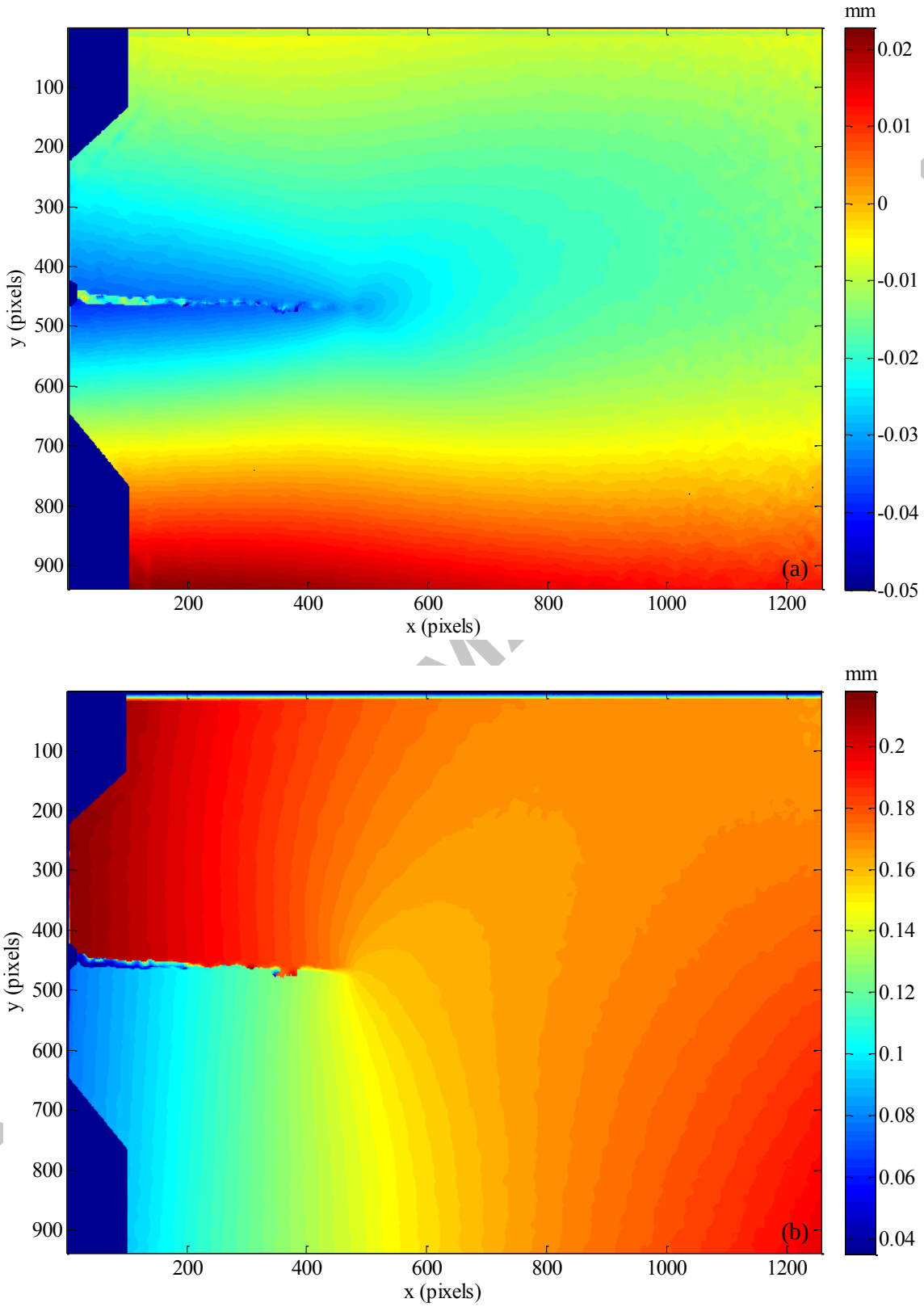

Figure 3 (a) Horizontal and (b) Vertical displacement fields measured with DIC for a crack length of 9.40 mm at a load level of 750 N.

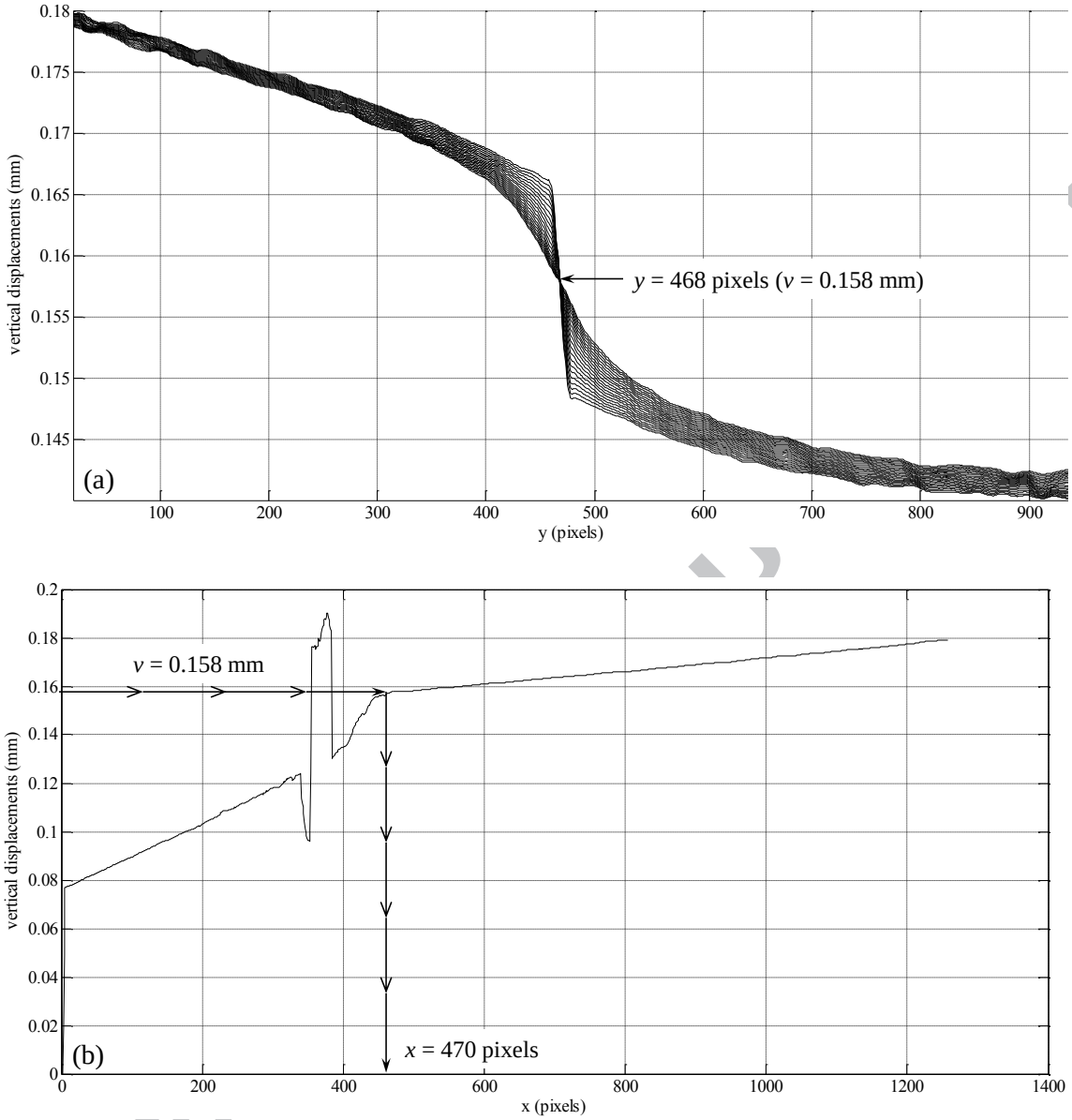

Figure 4 Graphs to support the explanation given in the paper of the methodology used for locating the crack tip: (a) *y*-coordinate and (b) *x*-coordinate.

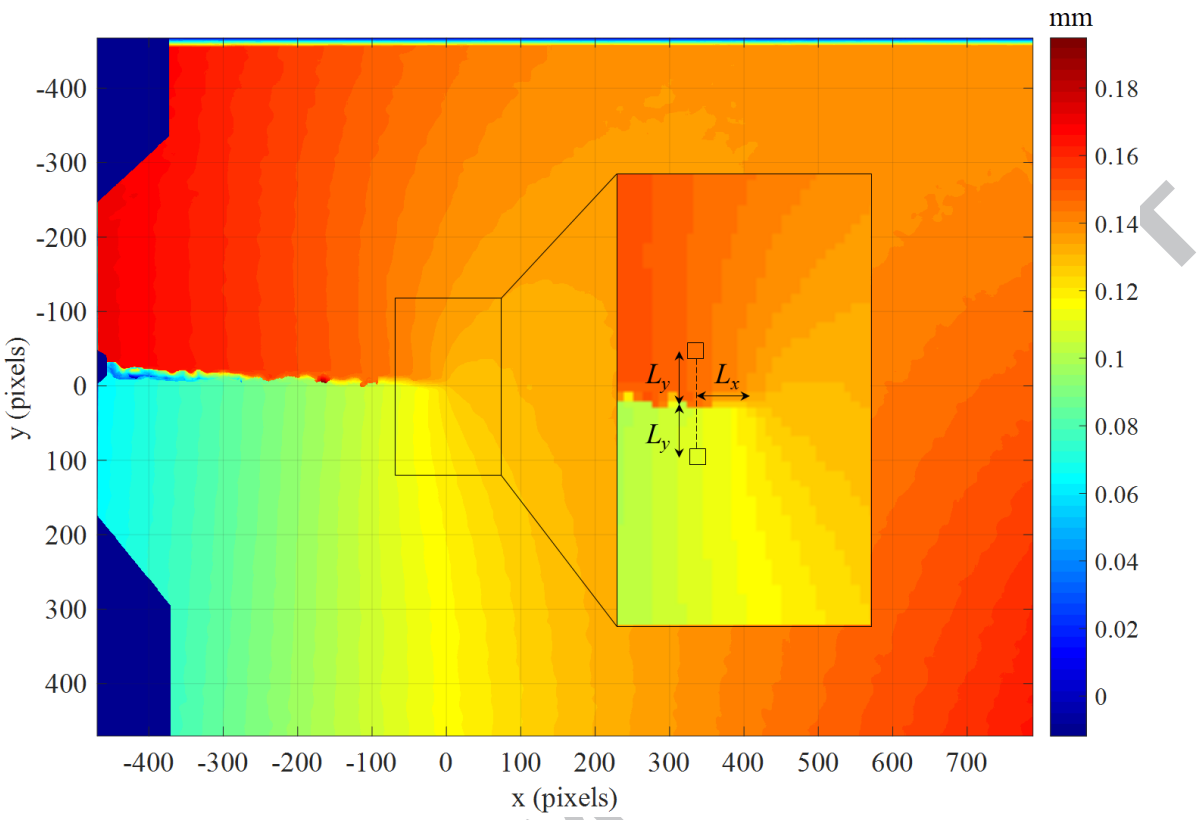

Figure 5 Magnified view of the crack tip region illustrating how CTOD measurements are based on a particular pair of points behind the crack tip. The coordinate axes have been modified with their origin at the crack tip.

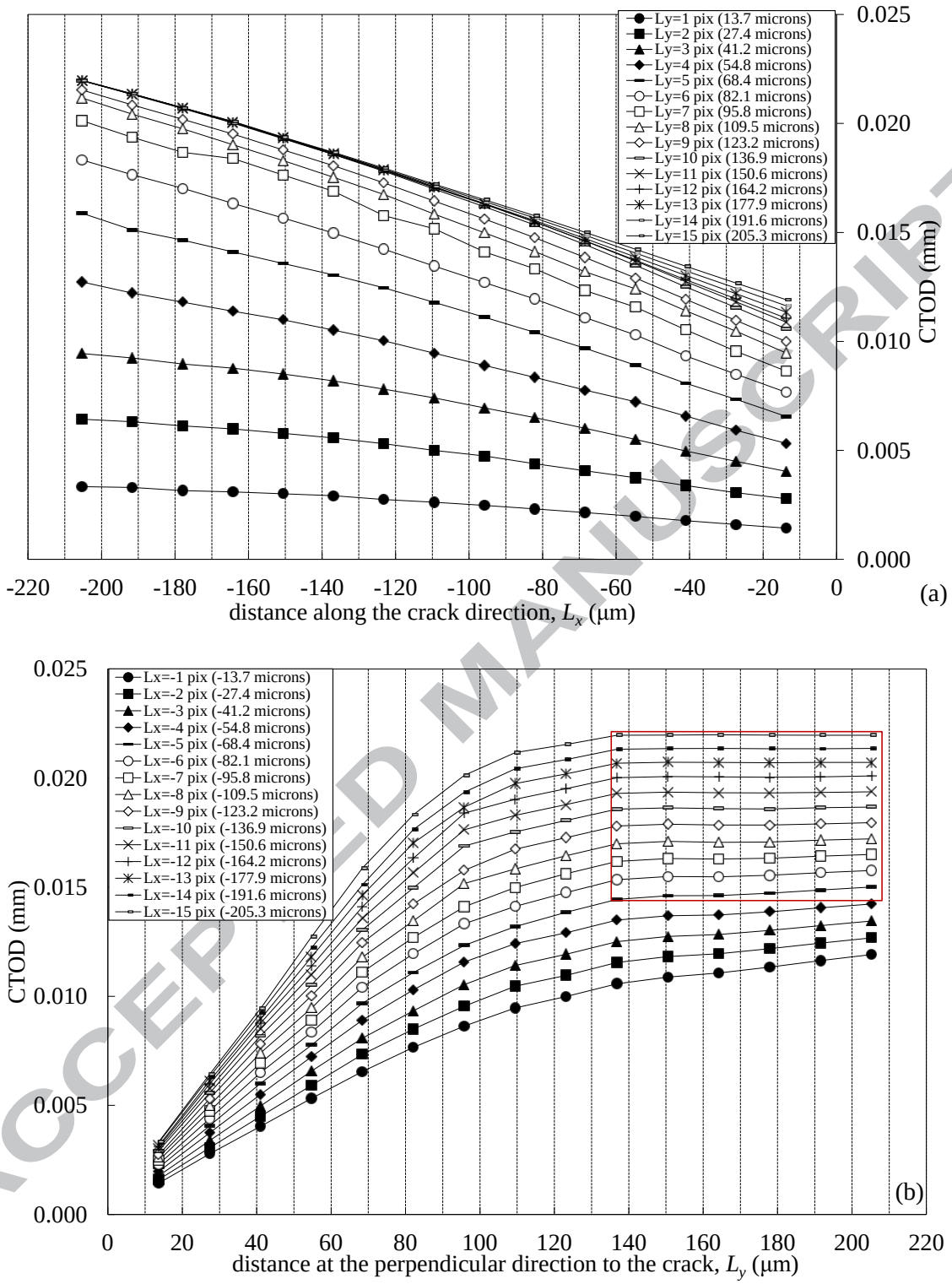

Figure 6 Graphs showing the effect of the location behind the crack tip of the selected points used for the CTOD measurement. (a) As a function of the distance along the crack plane L_x; (b) As a function of the distance in the perpendicular direction L_y to the crack plane.

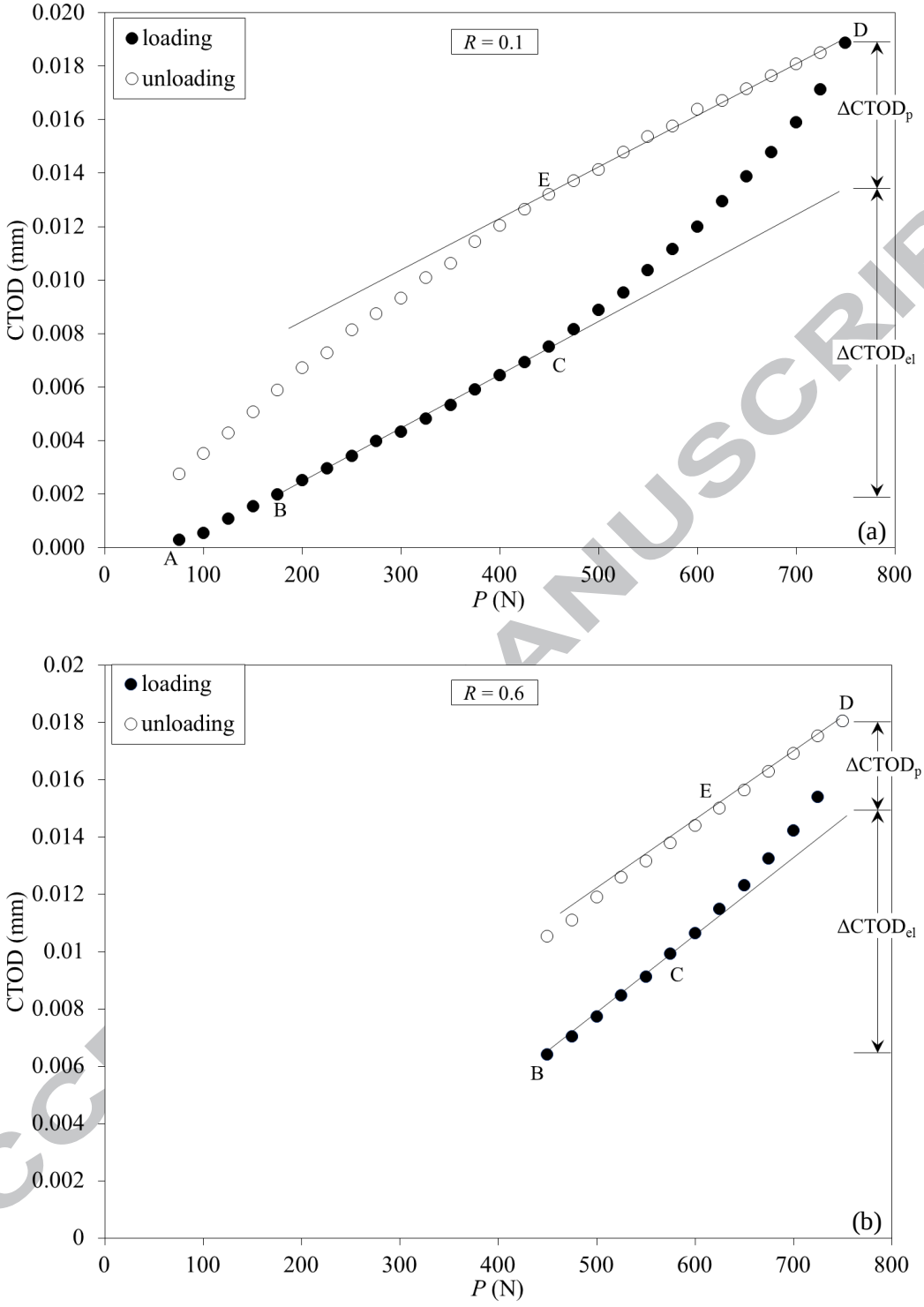

Figure 7 Plot of CTOD through a complete loading cycle, showing its elastic and plastic components at a crack length of 9.40 mm for the specimen tested at R =0.1 (a) and 9.20 mm for the specimen tested at R = 0.6 (b) using 5 pixels (68.4 μm) and 10 pixels (136.8 μm) for the distances L_x and L_y, respectively.

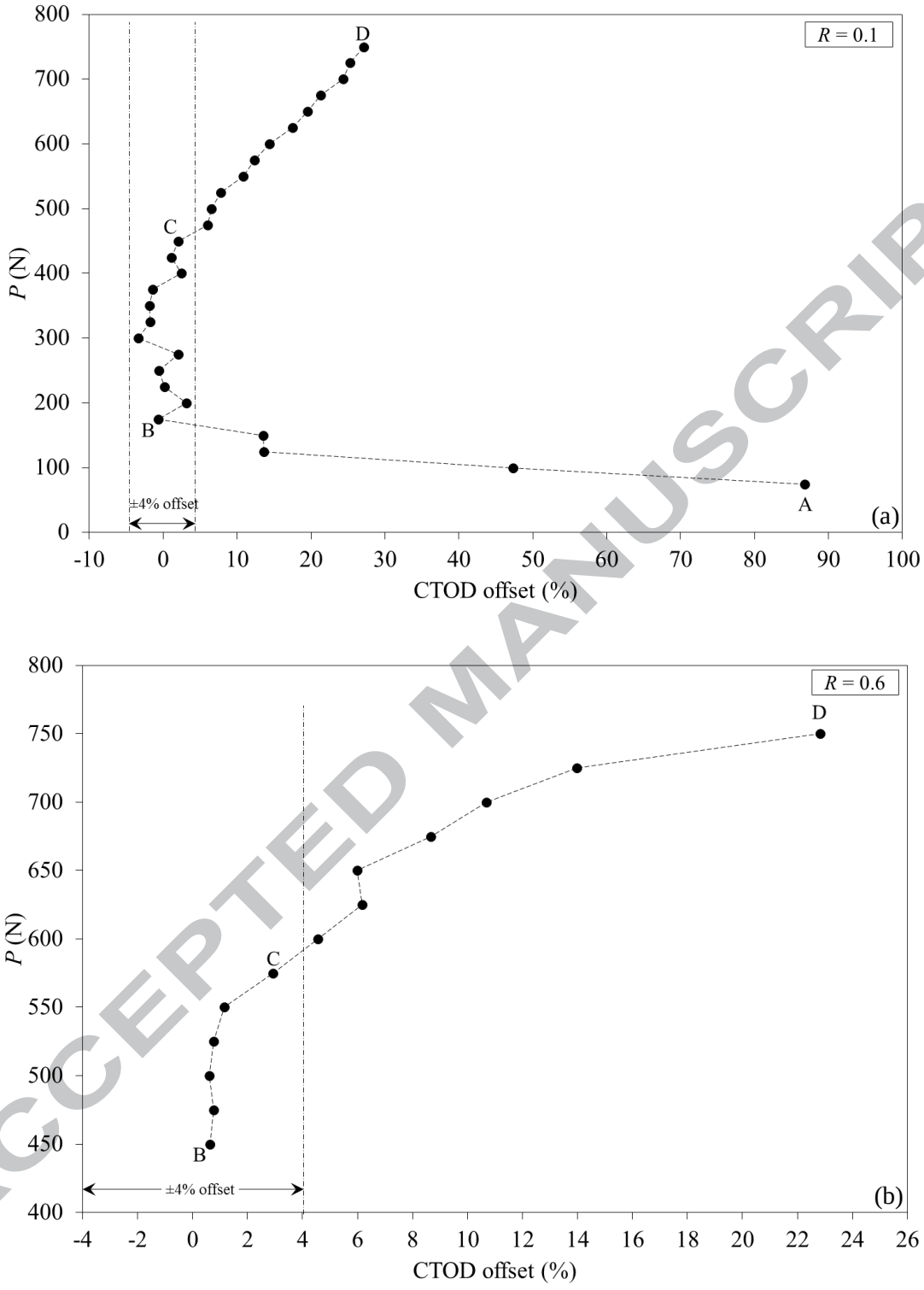

Figure 8 Variation of CTOD offset as a function of the applied load at a crack length of 9.40 mm for the specimen tested at R = 0.1 (a) and 9.20 mm for the specimen tested at R = 0.6 (b). A value of 4% was set as the offset criterion to define the region of the curve corresponding to the elastic component of the CTOD.

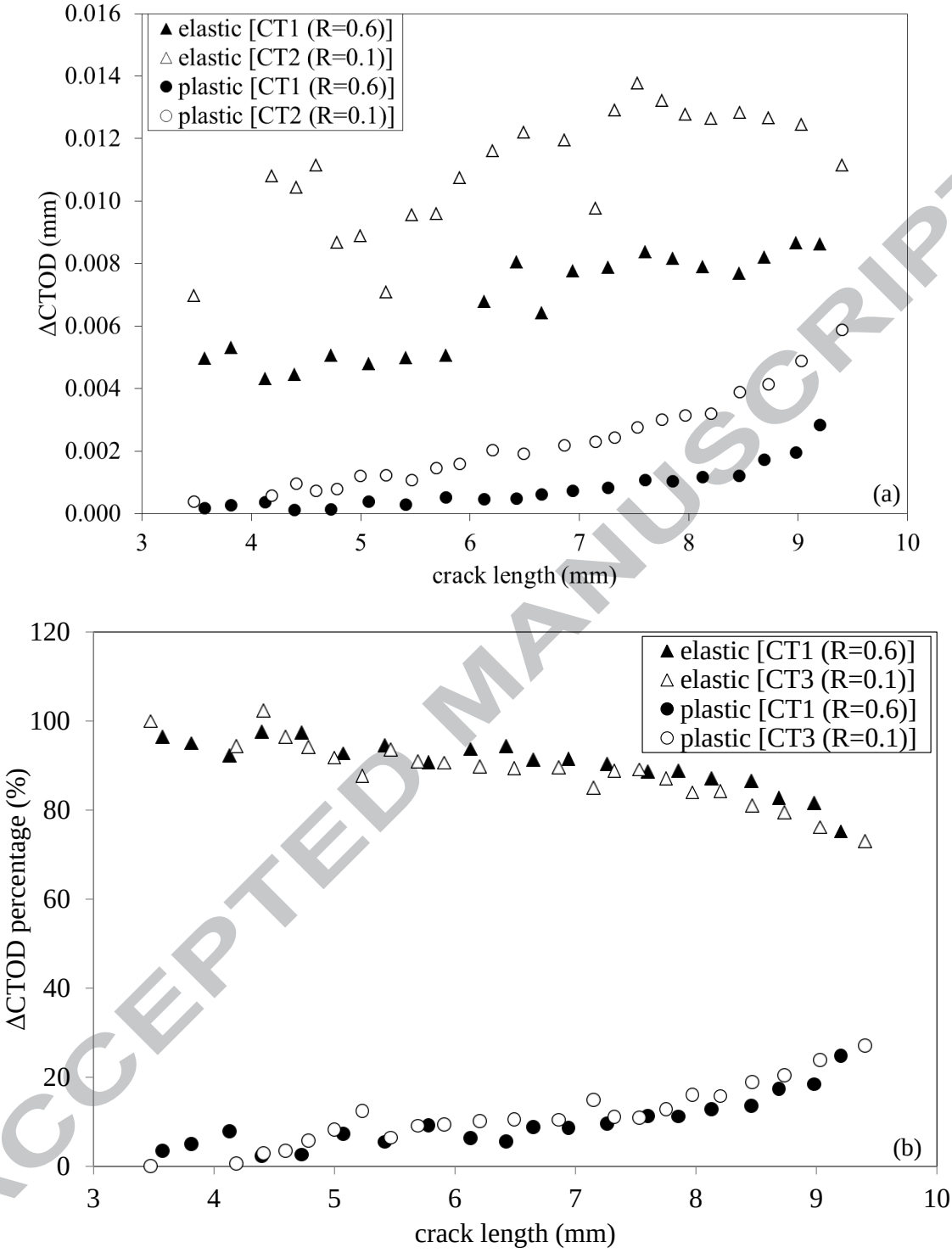

Figure 9 (a) Elastic and plastic CTOD ranges as a function of the crack length for both tests. (b) Elastic and plastic CTOD ranges as a percentage of the total CTOD range as a function of crack length.

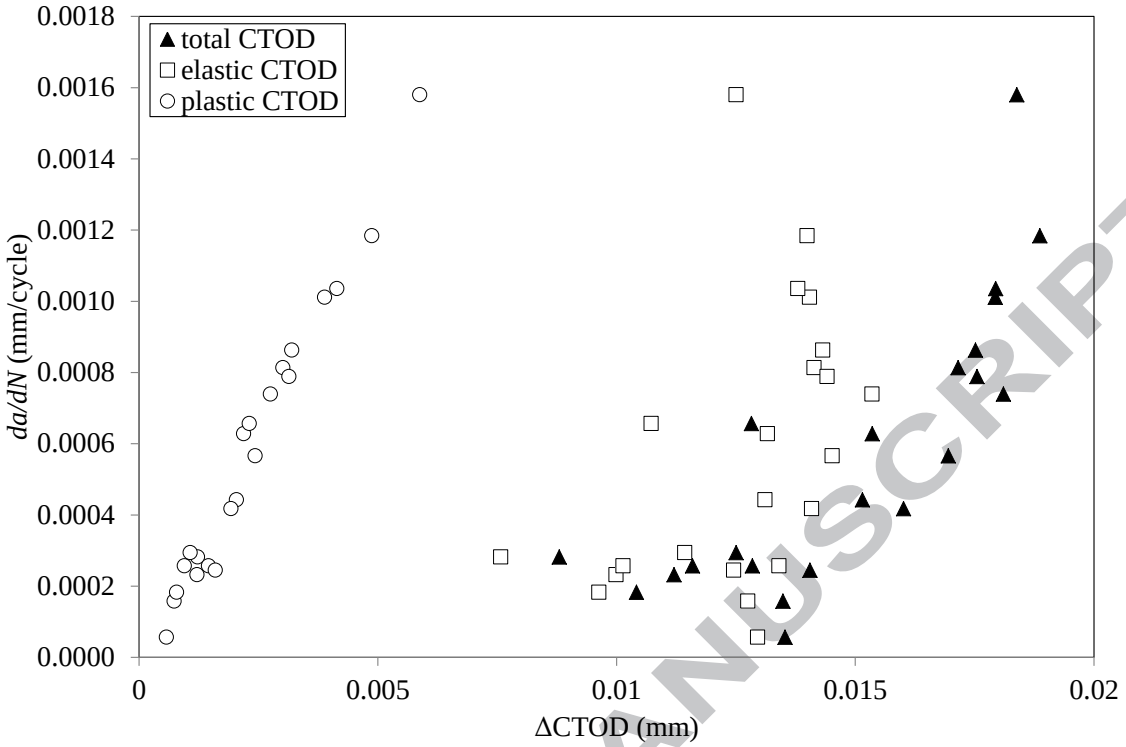

Figure 10 Crack growth rate per cycle (*da/dN*) as a function of the range of total CTOD ($\Delta CTOD_t$), elastic CTOD ($\Delta CTOD_{el}$) and plastic CTOD ($\Delta CTOD_p$) for the specimen tested at low stress ratio (R = 0.1).

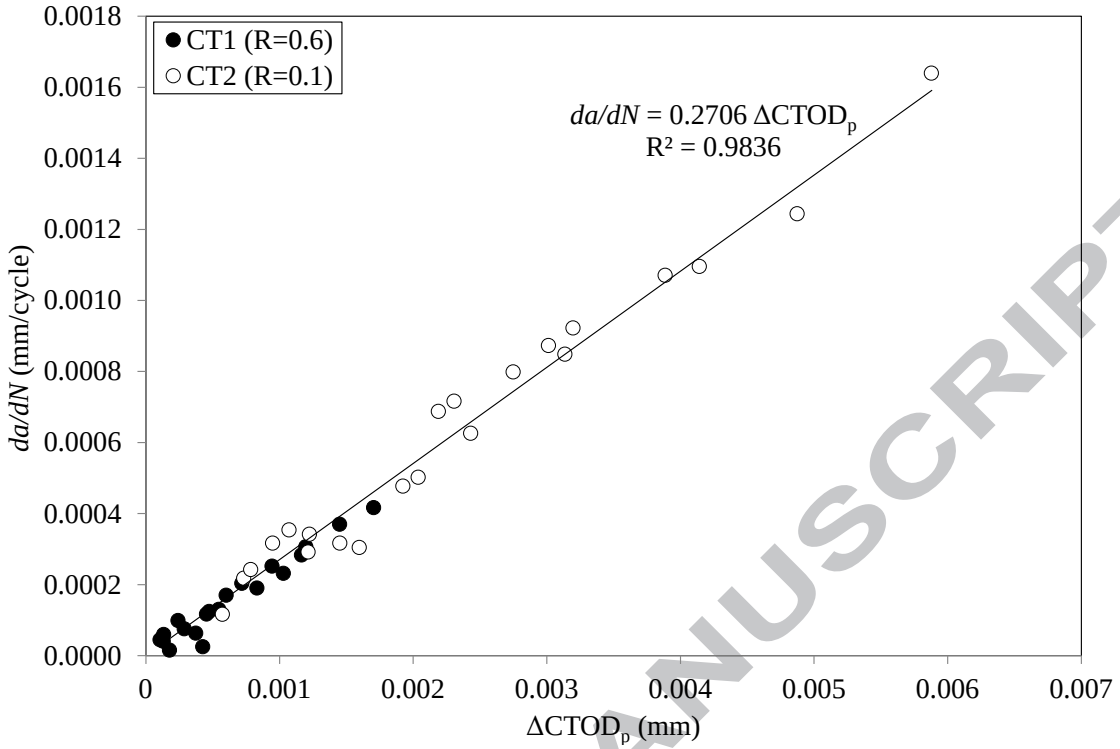

Figure 11 Plot of *da/dN* versus $\Delta CTOD_p$ for the two tests conducted at low (R = 0.1) and high (R = 0.6) stress ratio values.

Highlights:

- Characterisation of fatigue crack growth by using CTOD.
- Experimental measurement of CTOD using DIC.
- CTOD resolved into elastic and plastic components.
- Linear correlation between fatigue crack growth and the plastic CTOD range.
- CTOD as a useful alternate characterising parameter of fatigue crack growth.